



# Medium-density amorphous ice unveils shear rate as a new dimension in water's phase diagram

Ingrid de Almeida Ribeiro<sup>a</sup> , Debdas Dhabal<sup>a,1</sup> , Rajat Kumar<sup>a</sup>, Suvo Banik<sup>b,c</sup>, Subramanian K. R. S. Sankaranarayanan<sup>b,c</sup>, and Valeria Molinero<sup>a,2</sup>

Affiliations are included on p. 8.

Edited by Pablo Debenedetti, Princeton University, Princeton, NJ; received July 17, 2024; accepted October 9, 2024

Recent experiments revealed a new amorphous ice phase, medium-density amorphous ice (MDA), formed by ball-milling ice  $I_h$  at 77 K [Rosu-Finsen *et al.*, *Science* 379, 474–478 (2023)]. MDA has density between that of low-density amorphous (LDA) and high-density amorphous (HDA) ices, adding to the complexity of water's phase diagram, known for its glass polyamorphism and two-state thermodynamics. The nature of MDA and its relation to other amorphous ices and liquid water remain unsolved. Here, we use molecular simulations under controlled pressure and shear rate at 77 K to produce and investigate MDA. We find that MDA formed at constant shear rate is a steady-state nonequilibrium shear-driven amorphous ice (SDA), that can be produced by shearing ice  $I_h$ , LDA, or HDA. Our results suggest that MDA could be obtained by ball-milling water glasses without crystallization interference. Increasing the shear rate at ambient pressure produces SDAs with densities ranging from LDA to HDA, revealing shear rate as a new thermodynamic variable in the nonequilibrium phase diagram of water. Indeed, shearing provides access to amorphous states inaccessible by controlling pressure and temperature alone. SDAs produced with shearing rates as high as  $10^6 \text{ s}^{-1}$  sample the same region of the potential energy landscape than hyperquenched glasses with identical density, pressure, and temperature. Intriguingly, SDAs obtained by shearing at  $\sim 10^8 \text{ s}^{-1}$  have density, enthalpy, and structure indistinguishable from those of water “instantaneously” quenched from room temperature to 77 K over 10 ps, making them good approximants for the “true glass” of ambient liquid water.

water | amorphization | glasses | shear | polyamorphism

Recently, Rosu-Finsen *et al.* ball-milled ice  $I_h$  at 77 K, producing a new amorphous phase with a density of  $1.06 \pm 0.06 \text{ g cm}^{-3}$  upon recovery at 0.1 MPa (1). This new phase has been designated as medium-density amorphous ice (MDA) because its density falls between the  $0.94 \pm 0.02 \text{ g cm}^{-3}$  of low-density amorphous ice (LDA) and  $1.16 \pm 0.03 \text{ g cm}^{-3}$  of high-density amorphous ice (HDA) relaxed to atmospheric pressure (2–6). This finding adds to the intricacy of water's phase diagram (7–9), which is renowned for its glass polyamorphism (3, 10–13), and two-state thermodynamics (14–16) characterized by the possibility of coexistence between low-density (LDL) and high-density (HDL) liquid phases (17). It has been conjectured that MDA could be the genuine glassy state of ambient liquid water, a heavily sheared crystalline material, or an amorphous state more stable than LDA and HDA in some range of temperatures and pressures (1). To date, the true nature of MDA and its relationship with other amorphous water states remain elusive.

During the ball-milling process, ice is compressed and sheared in an uncontrolled manner. Rosu-Finsen *et al.* showed that molecular simulations with TIP4P/Ice that subject ice  $I_h$  to a sequence of random layer displacements followed by energy minimization produce an amorphous solid with density  $0.97 \text{ g cm}^{-3}$  and peaks in the structure factor close to those of MDA in the experiments (1). However, the pathway of amorphization in those simulations is unphysical, and could not address how MDA forms on ball-milling nor how its properties depend on pressure and shear rate. Here, we use molecular simulations with the TIP4P/Ice (18) and ML-BOP (19) water models at controlled temperature, pressure, and shear rate (*SI Appendix, sections I and II*) to investigate the formation and properties of MDA, and its relationship to the liquid and amorphous solid states of water.

## Results and Discussion

**MDA Is a Shear-Driven Amorphous (SDA) State.** Ball-milling involves both shearing and compression. We simulate the ball-milling of ice by subjecting polycrystalline ice  $I_h$  at 77 K to shear deformation at 0.1 and 250 MPa. We shear polycrystalline cells with  $\frac{1}{2}$  million ML-BOP water molecules partitioned in five  $\sim 15 \text{ nm}$  ice grains (Fig. 1A) or five hundred

## Significance

Water can form two noncrystalline solids by modulating temperature and pressure: low-density and high-density amorphous ices (LDA and HDA), regarded as glasses of distinct liquid phases. Recently, a medium-density amorphous ice (MDA) with density close to ambient liquid water was produced by ball-milling ice  $I_h$ , raising questions about its relation to other water phases. Our study reveals that MDAs with densities from LDA to HDA are obtained by increasing the shear rate, highlighting the role of shear in accessing unique amorphous states, including solids indistinguishable from instantaneously quenched liquid water, that cannot be obtained by controlling only temperature and pressure. This finding has broader implications for other tetrahedral substances like silicon and silica, which share similar thermodynamic behaviors with water.

Author contributions: V.M. designed research; I.d.A.R., D.D., R.K., S.B., S.K.R.S.S., and V.M. performed research; I.d.A.R. and V.M. analyzed data; and I.d.A.R. and V.M. wrote the paper.

The authors declare no competing interest.

This article is a PNAS Direct Submission.

Copyright © 2024 the Author(s). Published by PNAS. This article is distributed under [Creative Commons Attribution-NonCommercial-NoDerivatives License 4.0 \(CC BY-NC-ND\)](https://creativecommons.org/licenses/by-nc-nd/4.0/).

<sup>1</sup>Present address: Department of Chemistry, Indian Institute of Technology, Guwahati, Assam 781039, India.

<sup>2</sup>To whom correspondence may be addressed. Email: Valeria.Molinero@utah.edu.

This article contains supporting information online at <https://www.pnas.org/lookup/suppl/doi:10.1073/pnas.2414444121/-/DCSupplemental>.

Published November 22, 2024.

$\sim 3$  nm ice grains (Fig. 1B) at a shear rate  $\dot{\gamma} = 10^8 \text{ s}^{-1}$ . While this  $\dot{\gamma}$  is likely higher than the typically 10 to  $10^3 \text{ s}^{-1}$  (20) estimated to be accessible through ball-milling, it enables the computational study of ice amorphization using large-scale simulations. Shearing of the cell with  $\sim 15$  nm grains at both 0.1 and 250 MPa results in amorphization of  $1/3$  of the ice, while almost  $3/4$  of the 3 nm ice grains are amorphized upon shearing (Table 1 and *SI Appendix, Fig. S1*). The latter is comparable to the  $69 \pm 5\%$  amorphization reported from the experiments (1). The extent of amorphization in the simulations seems to plateau upon shearing (*SI Appendix, Fig. S1*), consistent with the experiments (1) and the  $t^{1/2}$  growth of the width of the disordered layer in mechanical amorphization (21).

The simulations reveal that the pathway of amorphization involves both grain-boundary sliding (25) (GBS) and the breaking of crystallites. The latter is only observed for the  $\sim 15$  nm crystals, increasing the number of ice grains with time (*SI Appendix, Fig. S2*). However, the nanoscopic size of the initial crystallites in our simulations makes GBS the main mechanism of plastic deformation, and the exclusive one for the cell with  $\sim 3$  nm grains. We anticipate that amorphization due to dislocation-induced structural changes dominates in the early stages of ball-milling of macroscopic ice crystals and GBS in the later stages of plastic deformation of ice to produce MDA.

The density of the amorphous state produced by shearing increases with the shearing pressure and is independent of the initial size of the ice grains (Table 1). Most importantly, the amorphous region has density  $0.99 \pm 0.01 \text{ g cm}^{-3}$  when shearing at 0.1 MPa and  $1.10 \pm 0.02 \text{ g cm}^{-3}$  at 250 MPa, intermediate between the ones of HDA and LDA. The latter is the most stable amorphous ice for ML-BOP for pressures below 410 MPa at 77 K (26). The density of the amorphous states produced in the shearing simulations at 0.1 and 250 MPa agree with the lower and upper estimates for MDA from the experiments  $1.06 \pm 0.06 \text{ g cm}^{-3}$  (1) (Table 1). We conclude that MDA is a truly distinct nonequilibrium SDA state of water, distinct from LDA and HDA.

**MDA Can Be Obtained by Shearing LDA or HDA.** The presence of ice crystallites poses a challenge to the characterization of MDA. A minimum of 30% crystallinity persists after 80 cycles of ball-milling in the experiments (1), raising the question of whether MDA could be synthesized through ball-milling of amorphous samples, eliminating ice contributions to the measurements.

We subject HDA and LDA modeled with ML-BOP and TIP4P/Ice to shear deformation at 77 K while applying different pressures and shear rates (*SI Appendix, section III*) and perform GBS amorphization of ice with the TIP4P/Ice model at the same

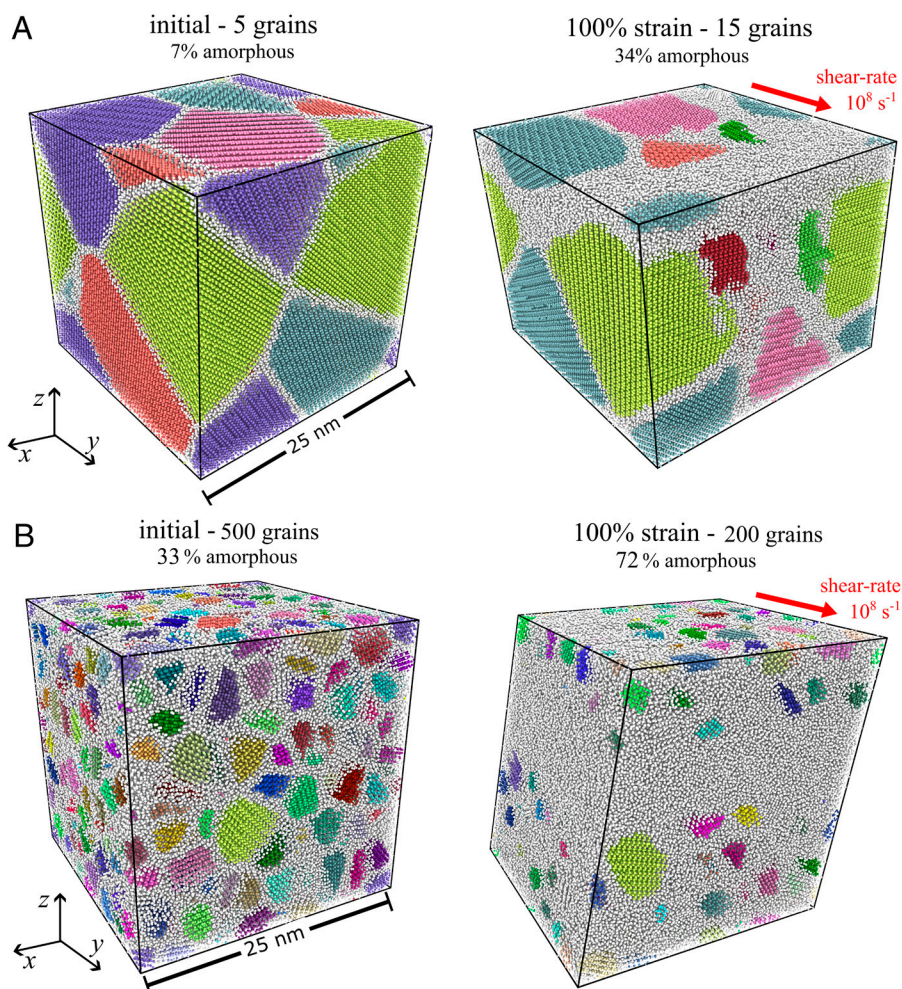


**Fig. 1.** MD simulation snapshots of polycrystalline ice samples. We start with (A) five ice grains, each about 15 nm in size or (B) with approximately 500 ice grains, with an average size of 3 nm. These grains are represented by different colors, indicating their orientations, while the gray spheres denote disordered regions. To identify the ice grains, we use the grain segmentation algorithm implemented in Ovito (22, 23). The total amount of amorphous and ice are identified by CHILL+ (24). Subsequently, we reach the configuration equivalent to a strain of  $\gamma = 1$ , at which the density has become stationary. We define  $\gamma = L_{yz}/L_z$ , where  $L_{yz}$  is the change in length along the shearing direction and  $L_z$  is the initial length of the box. The shear deformation is imposed at a constant shear rate of  $\dot{\gamma} = 10^8 \text{ s}^{-1}$ . See *SI Appendix, sections I and II* for details.

conditions (*SI Appendix, section IV*). While recrystallization under shear hinders the complete amorphization of ice I, we do not detect ice formation upon shearing of glasses at 77 K (*SI Appendix, Table S1*), even for ML-BOP that readily crystallizes in cooling simulations (19, 26, 27) (*SI Appendix, Table S1*). Fig. 2 shows that the density of MDA obtained by shearing ice  $I_b$  (blue squares), LDA (cyan triangles), and HDA (red circles) at  $\dot{\gamma} = 10^8 \text{ s}^{-1}$  are identical. That is also the case for the fraction of four-coordinated molecules  $f_4$  (*SI Appendix, Figs. S6 and S7*) and the energy (*SI Appendix, Figs. S8 and S9*) of the SDA states. Despite the high shear rates, there are no signs of anisotropy in the structure of the SDAs (*SI Appendix, Fig. S6*). We conclude that the properties of the SDA state depend on temperature, pressure, and shear rate but are independent from the parent state.

The lack of memory of the initial state in the properties of MDA is consistent with the recovery of time translation invariance for glasses under constant shear (30, 31). SDA obtained under constant shear are nonequilibrium stationary states (NESS) characterized by the intensive variables that define the equilibrium state of the one component systems,  $p$  and  $T$ , plus the shear-rate  $\dot{\gamma}$  that keeps the system out of equilibrium (Fig. 3). Because the SDAs are NESS, they can be considered thermodynamically well-defined nonequilibrium phases. Consistent with the stationary nature of the SDAs, *SI Appendix, section VIII* shows that SDAs with same  $p$ ,  $T$ , and  $\dot{\gamma}$  obtained by isochoric or isobaric shearing are identical. The recovery of time invariance under constant shear makes the SDA distinct from LDA, HDA, and hyperquenched glasses (HQGs), which are history-dependent, nonstationary states. In what follows, we characterize the SDA phases obtained by steady shearing of ML-BOP and TIP4P/Ice glasses at 77 K, the temperature of the ball-milling experiment, and their relation to LDA, HDA, and liquid water.

**Density of MDA Spans All the Range from LDA to HDA.** We characterize the properties of the sheared-driven amorphous phases produced with shear rates encompassing 8 orders of magnitude, from  $\dot{\gamma} = 10^5$  to  $10^{12} \text{ s}^{-1}$ , at 77 K and pressures from 0.1 to 700 MPa. Fig. 2 *A* and *C* reveal that the density of the SDA increases with the shear rate, spanning all the range from LDA to HDA.

The density range of the shear-driven phase is broadest at 0.1 MPa, and decreases with pressure, becoming almost independent of  $\dot{\gamma}$  at 700 MPa (Fig. 2 *C*). On the contrary, the energy and enthalpy of the sheared phase monotonously increase with  $\dot{\gamma}$  (*SI Appendix, Fig. S11 B and D*), even at the highest pressures for which the density is insensitive to shearing. We conclude that having a “medium density” is not the defining characteristic of the shear-driven phases. In what follows, we use indistinctly SDA or MDA to refer to the sheared nonequilibrium amorphous phase.

The densities of SDAs prepared at the lowest shear,  $\dot{\gamma} = 10^5 \text{ s}^{-1}$  in our simulations, approach those of the most stable amorphous state: LDA at low pressures and HDA at high ones (Fig. 2 *A*), as

expected from the  $T$ - $p$ - $\dot{\gamma}$  phase diagram sketched in Fig. 3. Notably,  $\rho(p)$  of the SDA produced at  $\dot{\gamma} = 10^5 \text{ s}^{-1}$  (red crosses in Fig. 2 *A*) follows the “S-shaped” curve of glasses produced by isobaric cooling (purple line in Fig. 2 *A*). The S-shaped  $\rho(p)$  of these steady-state SDAs reveals signatures of the liquid–liquid transition (LLT) of the water model (26), albeit as a continuous transformation.

In contrast, the  $\rho(p)$  curves of SDAs produced at higher shear rates show no inflection point (see red circles and red diamonds in Fig. 2 *A* for  $\dot{\gamma} = 10^8$  and  $10^{12} \text{ s}^{-1}$ ) signaling that all remnants of a liquid–liquid transformation disappear under strong shearing as the liquid adopts a uniformly higher density across all pressures. Based on the energetics of SDA discussed below, we interpret that increasing the shear rate results in sampling of regions of the potential energy landscape increasingly higher above the megabasins of LDA and HDA, where the distinction between the two phases disappears.

**MDA Is Never More Stable than Both LDA and HDA.** To understand the energetics of the SDA phases, we first determine the enthalpy of crystallization  $\Delta H_{\text{cryst}}$  of MDA recovered in the experiment, dividing the experimental enthalpy of crystallization of the ball-milled ice,  $-1.21 \pm 0.15 \text{ kJ mol}^{-1}$  by the  $69 \pm 5\%$  amorphous fraction of the sample (1). The resulting  $\Delta H_{\text{cryst}}$  of recovered MDA is  $-1.75 \pm 0.13 \text{ kJ mol}^{-1}$ , intermediate between  $\Delta H_{\text{cryst}}$  of LDA ( $-1.35 \pm 0.15 \text{ kJ mol}^{-1}$ ) and HDA ( $-2.01 \pm 0.15 \text{ kJ mol}^{-1}$ ) (34–36). We conclude that not only the density, but also the enthalpy of MDA obtained in the experiment is intermediate between the ones of the high- and low-density water glasses. In what follows, we use simulations to address how does the enthalpy of MDA evolve with the shear rate and pressure at 77 K.

The enthalpy of the SDA phases decreases with lowering shear rate, asymptotically approaching the enthalpy of the more stable glass at the corresponding pressure, LDA, or HDA (*SI Appendix, Fig. S11 D*). Indeed, there is no pressure for which SDA has lower enthalpy than both LDA and HDA (Fig. 2 *D*), supporting that amorphous phases of intermediate density are always less stable than low- and high-density amorphous ices (37).

Shearing of glasses typically results in rejuvenation (38–40), i.e. an increase in potential energy through plastic deformation, because both enthalpy and energy increase with the shear rate (*SI Appendix, Fig. S11*). However, Fig. 2 *D* evinces a range of SDAs with enthalpy intermediate between LDA and HDA. The formation of those SDAs from the least stable amorphous ice proceeds with decrease in energy, akin to aging of the glass. Aging through plastic deformation has been previously reported only upon cyclic shearing (39, 40). The polyamorphism of water enables aging through steady shear of the least stable amorphous ice.

SDA produced at 77 K and  $\dot{\gamma} = 10^8 \text{ s}^{-1}$  has enthalpy  $\sim 6 \text{ kJ mol}^{-1}$  lower than the liquid at  $T_m$  (Fig. 2 *D*), despite having the same density (Fig. 3 *A* and *B*). Interestingly, at all pressures from 0.1 to 700 MPa the enthalpy of SDA prepared at  $\dot{\gamma} = 10^8 \text{ s}^{-1}$  (red circles in Fig. 2 *D*) is the same as that of HDA, despite the large

**Table 1. Density measurements at  $T = 77 \text{ K}$  for different pressures, where  $\rho_{\text{total}}$  is the total density and  $\rho_{\text{MDA}}$  is the density of the amorphous region**

	Load pressure (MPa)	Initial average grain size (nm)	$\rho_{\text{total}}$ ( $\text{g cm}^{-3}$ )	% amorphous	$\rho_{\text{MDA}}$ ( $\text{g cm}^{-3}$ )
Exp. ref. 1	unknown (recovered at 0.1)	macroscopic	$1.02 \pm 0.03$	$69 \pm 5$	$1.06 \pm 0.06$
MD	250	3	$1.05 \pm 0.01$	72	$1.09 \pm 0.01$
MD	250	15	$1.01 \pm 0.01$	34	$1.11 \pm 0.01$
MD	0.1	15	$0.96 \pm 0.01$	33	$0.99 \pm 0.01$

The volume occupied by MDA was estimated using  $V_{\text{MDA}} = (V_{\text{total}} - n_{\text{ice}}V_{\text{ice}})/n_a$ , where  $n_a$  is the amorphous fraction. We use CHILL+ to identify ice (24). *SI Appendix, Fig. S1C* shows the evolution of the density of the amorphous region during the shearing process.

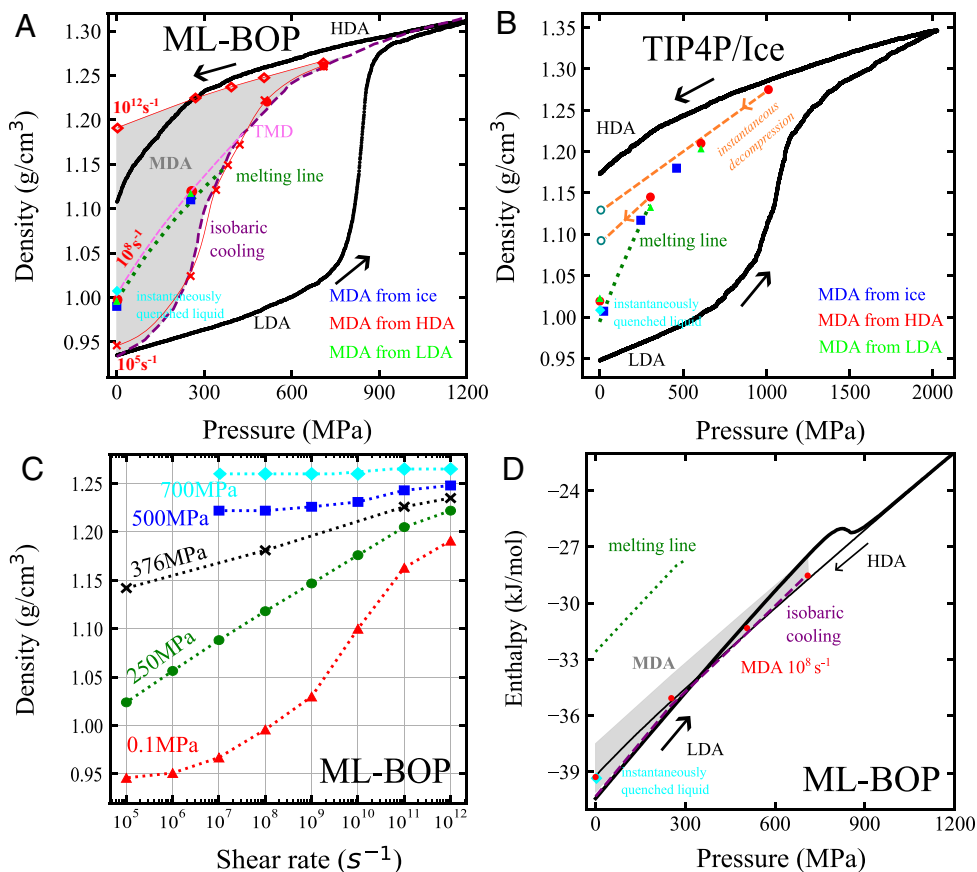


**Fig. 2.** Density of and enthalpy of the SDA ices prepared at 77 K at constant shear rate and pressure. Panels (A) and (B) present the density as a function of pressure for amorphous phases of ML-BOP and TIP4P/Ice at 77 K. The densities of SDAs produced by shearing at a constant shear rate of  $\dot{\gamma} = 10^8 \text{ s}^{-1}$  ice are shown with blue squares, by shearing LDA with green triangles, and by shearing HDA with red circles. The green dotted line is the density of the liquid obtained along the melting line  $T_m$  without applied shear (27, 28). The dashed magenta line in (A) indicates the density of the liquid at the TMD under no shear. The cyan diamonds in (A), (B), and (D) indicate the density and absolute enthalpy of the glass produced by instantaneous quenching of liquid water from 280 K to 77 K at 0.1 MPa. The gray region in (A) encompasses all SDAs made by shearing at  $\dot{\gamma}$  from  $10^5 \text{ s}^{-1}$  to  $10^{12} \text{ s}^{-1}$  (SI Appendix, Figs. S10 and S11); the red crosses and red diamonds show the data at the slowest and fastest shear rates at the lower and upper boundaries, respectively. The purple dashed line in (A) represents the density of the hyperquenched glass (HQG) after isobarically cooling the liquid at  $10 \text{ K ns}^{-1}$  (29). The black lines correspond to the compression-induced LDA-to-HDA transformation and decompression of HDA, all at 77 K in the absence of shear. The empty teal circles in panel (B) show the density upon instantaneous decompression of high-pressure SDAs to which they are connected by dashed orange arrows. (C) Density of SDAs of ML-BOP as a function of shear rate at various pressures. (D) Enthalpy of the SDAs obtained by shearing ML-BOP. The gray area represents all the range of enthalpies of SDAs sheared at rates  $10^5 \text{ s}^{-1}$  to  $10^{12} \text{ s}^{-1}$ , the SDAs produced by shearing at  $10^8 \text{ s}^{-1}$  (red circles) have the same enthalpy as HDA (thin black line). The enthalpy of LDA is shown with a thick black line, the enthalpy of the liquid at the melting line with a green dashed line, and the enthalpy of the hyperquenched glasses produced by isobaric cooling of the liquid at  $10 \text{ K ns}^{-1}$  by a dashed purple line. We find that the enthalpy of HQG is quite similar to that of the most stable LDA and HDA states, indicating that hyperquenching can produce more stable glasses compared to compression/expansion at 77 K. The simulation details are presented in SI Appendix, sections II, III, and IV.

difference in density between those amorphous states (Fig. 2 A and B). We conclude that shear-driven phases have distinct energy-density relations than previously known amorphous ices.

While the density of SDAs is essentially bound by those of LDA and HDA, SDAs produced at high shearing rates have higher enthalpy than both LDA and HDA (Fig. 2D). As we discuss in next section, these high energy states can only be accessed through shearing.

**Shearing Provides Access to Amorphous States That Cannot Be Reached by Hyperquenching.** In the absence of shear, supercooled ML-BOP and TIP4P/Ice exhibit a LLT with a critical point around 170 MPa and 180 K (Fig. 3) (26, 33, 41). Fig. 4 presents a sketch of the amorphous  $\rho$ - $p$  phase diagram at 77 K of water or a water model that has a LLT. The figure presents the  $\rho(p)$  of the hypothetical equilibrium LDL and HDL phases at 77 K and their first-order transition (dashed black lines), as well as the  $\rho(p)$  of the SDA produced with three distinct shear rates (thin black lines) to illustrate the smoothing and disappearance of all signatures of the LLT with

increased shearing rate. The different colors in the figure illustrate the regions of amorphous states accessible by either hyperquenching or shearing (blue area), exclusively through shearing (magenta area), and only through hyperquenching (gray area). In what follows, we discuss what sets the boundaries of these regions.

The existence of a maximum density in liquid water provides an upper bound  $\rho_{\text{max}}(p)$  for the density of hyperquenched glasses in the LDL side of the phase diagram.  $\rho_{\text{max}}(p)$  is almost indistinguishable from the densities of SDAs prepared by shearing at  $\dot{\gamma} = 10^8 \text{ s}^{-1}$  for both ML-BOP and TIP4P/Ice (Fig. 2 A and B). The implication is that amorphous phases prepared by shearing these water models, and presumably also water, at rates below  $10^7 \text{ s}^{-1}$  have the same density of glasses obtained by hyperquenching (blue region in Fig. 4), while amorphous phases with  $\rho(p) > \rho_{\text{max}}(p)$  can only be accessed by shearing. In next section, we address whether the hyperquenched and sheared glasses with same  $p$ ,  $T$ ,  $\rho$  and  $\rho < \rho_{\text{max}}(p)$  are indistinguishable.

Cooling and shearing rates have opposite impacts on the density of the amorphous phases at pressures on the HDL side of

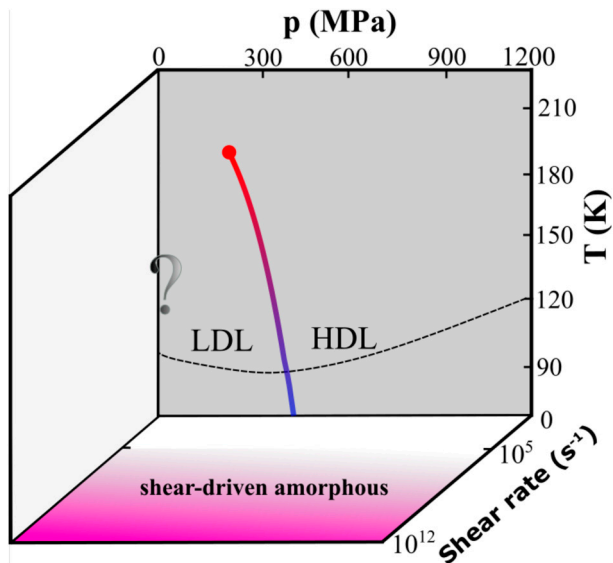


**Fig. 3.** Sketch of the  $T$ - $p$ - $\dot{\gamma}$  amorphous phase diagram of ML-BOP and TIP4P/Ice which have a LLT line at  $\dot{\gamma} = 0$  (blue to red colored line).  $p$  and  $T$  determine the phase behavior of the one component system in equilibrium. The application of a constant shear rate adds a new dimension to the phase diagram, producing distinct SDA nonequilibrium stationary states that may not be accessed through changes in temperature and pressure. The dashed black lines represent the glass transition temperatures  $T_g(p)$ , which have opposite slope for LDA and MDA in the models (26, 32) and experiments (7), and above which fast ice formation hinders the study of the LLT in water. The shaded magenta region represents the  $p, \dot{\gamma}$  area at 77 K, well below  $T_g(p)$ , investigated in this study. The sketch is based on data of the LLT of ML-BOP, which ends at a critical point located at  $170 \pm 10$  MPa and  $181 \pm 3$  K (26, 33). The equilibrium between LDL and HDL has been extrapolated to occur at  $p_{LL} = 410$  MPa at 77 K for ML-BOP (26). Similarly, the LLT of TIP4P/Ice has a critical point at  $173.9 \pm 0.6$  MPa and  $188.6 \pm 1$  MPa (34). Fig. 2 presents the density of the shear-driven phases at 77 K as a function of  $p$  and  $\dot{\gamma}$ . The question mark stresses the unknown impact of shear on the metastable LLT.

the phase diagram. The equilibrium density of HDL,  $\rho_{HDL}(p)$ , is approached from above by slower shearing (Fig. 2C) and from below by slower cooling (because the density of the liquid monotonously increases on cooling for pressures beyond the extremum of the line of maximum density,  $\rho_{max}(p_{max})$ , which for water occurs at  $\sim 150$  MPa (42) and for ML-BOP at  $p_{max} = 430$  MPa (SI Appendix, Fig. S12). These opposing trends of water density on cooling and shearing at high pressure result in disjoint regions for HQG and SDA (gray and magenta areas, respectively, in Fig. 4). The almost coincidence of the red cross and red diamond at 700 MPa in Fig. 2A indicates that the gap between the shear-driven and hyperquenching accessible regions in high pressure ML-BOP is negligible. This closeness originates in the high mobility of HDL in ML-BOP compared to water (26), and its resistance to crystallization into the high pressure ice polymorphs (27). We anticipate a larger gap between the regions accessible by shearing and hyperquenching of water in high-pressure experiments. We conclude that shearing can produce distinct nonequilibrium amorphous states of water that cannot be accessed by controlling only temperature and pressure.

**Are SDA Phases Identical to Hyperquenched Glasses with Same  $p, T, \rho$ ?** The existence of a  $\rho(p)$  region accessible to both SDA and HQG at 77 K (cyan area in Fig. 4) elicits the question of how similar are sheared and hyperquenched glasses that have identical  $p, T$ , and  $\rho$ . To address this, we first compare the SDA and HQG of ML-BOP prepared at 77 K and 300 MPa, both with a density of  $1.109 \text{ g cm}^{-3}$ . The SDA is made by shearing at  $\dot{\gamma} = 10^6 \text{ s}^{-1}$ , and the HQG by cooling the liquid at  $25 \text{ K ns}^{-1}$ . Despite the different methods used to obtain these amorphous phases, they exhibit

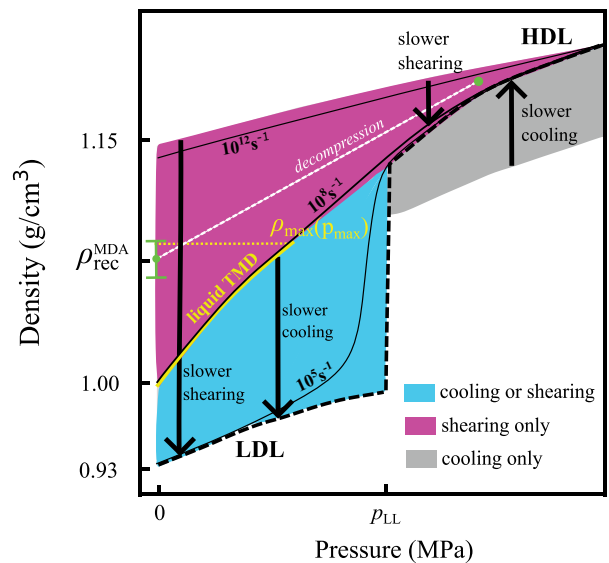


**Fig. 4.** Sketch of the density regions of the amorphous phases produced at 77 K under varying pressure and shear rates. The black dashed line refers to the hypothetical LDL and HDL at 77 K if these liquids could be equilibrated and ice crystallization could be avoided; the vertical dashed line indicates the first-order transition between these two phases. The blue area indicates the density region accessible via both shearing and cooling methods. We conjecture that the blue region may be fully reachable with slower shear rates and cooling rates. Conversely, the magenta region is exclusively accessible with high shear rates, as cooling the liquid is constrained by its maximum density (indicated by the yellow line). The density of HQG and SDA phases approach the density of the stable liquid, LDL, or HDL, when the cooling or shear rates are very slow (Fig. 2C), may be approaching the inverse of the relaxation time at 77 K. The thin black lines illustrate  $\rho(p)$  of the SDA at three different shear rates. The liquid-liquid coexistence temperature  $T_{LL}$  for water at 77 K in the absence of shear is expected to occur at  $p_{LL} \approx 250$  MPa (7), although it has also been proposed to occur at pressures below  $p_{max}$  (42). For ML-BOP at 77 K,  $p_{LL}$  is extrapolated to be at 410 MPa (26). Also in the absence of shear, the maximum (extremum) in the TMD to the newest equation of state of supercooled water (42) is  $\rho_{max} = 1.08 \text{ g cm}^{-3}$  at  $p_{max} = 151$  MPa and 177 K, while for ML-BOP  $\rho_{max} = 1.185 \text{ g cm}^{-3}$  at  $p_{max} = 430$  MPa and 128 K (SI Appendix, Fig. S12). At pressures above  $p_{max}$  the liquid does not display a density anomaly, and consequently the most stable state can be only reached by slower cooling rates. The white dotted line indicates the possible relaxation for MDA obtained in ball-milling experiments at high pressures to the experimentally recovered MDA with density  $1.07 \pm 0.02 \text{ g cm}^{-3}$ . Fig. 2C indicates that to reach such density at ambient pressure the shear rate should be  $\sim 10^{10} \text{ s}^{-1}$ , well above the rates reached by ball-milling.

identical structure factors  $S(q)$  (Fig. 5), enthalpies (SI Appendix, Fig. S13B), and have inherent structures with identical energies and densities (SI Appendix, Table S2).

Not only are the enthalpy and structure factors of these SDA and HQG samples identical at the same  $p, T$ , and  $\rho$  but so are their responses to compression and heating without any applied shear, as seen in SI Appendix, Figs. S13 A and B and S14A. Given that the heating and compression rates in these simulations may be too steep to enable significant aging, we further examine the evolution of the density and energy of these states as they age at 77 K and 300 MPa over 200 ns. SI Appendix, Fig. S13 C–F reveals less than 0.2% differences in the evolution of the glasses created by shearing and hyperquenching. The identical evolution of the glasses made by shearing and hyperquenching is consistent with them having the same inherent structures (SI Appendix, Table S2).

The results discussed above indicate that HQG and SDA produced with ML-BOP at 77 K and 300 MPa by cooling at  $25 \text{ K ns}^{-1}$  and shearing at  $10^6 \text{ s}^{-1}$ , respectively, are practically indistinguishable because they sample the same region of the potential energy landscape. This is unexpected, as  $p, T$ , and  $\rho$  do not generally suffice to fully determine the state of hyperquenched glasses (43–45). However, our finding that SDA prepared with

$\dot{\gamma} = 10^6 \text{ s}^{-1}$  and HQG obtained at  $25 \text{ K ns}^{-1}$  sample the same regions of the PEL is consistent with previous reports indicating that SPC/E glass obtained by cooling at  $30 \text{ K ns}^{-1}$  also samples the PEL of the corresponding liquid (45). Hence, the PEL sampled by these shear-driven and hyperquenched nonequilibrium amorphous solids would correspond to the one of the liquid at a well-defined higher fictive temperature (46, 47), enabling a description of the state of system with  $p$ ,  $T$ , and  $\rho$  (48, 49).

Vitrification of liquid water during the HDL to LDL transformation on cooling results in long-range structural correlations in the glass (26, 50). This is the case for the HQG produced by cooling ML-BOP to 77 K at  $25 \text{ K ns}^{-1}$  and 300 MPa. The long-range correlations in the  $S(q)$  of the HQG are exactly replicated in the MDA created by shearing HDA at  $\dot{\gamma} = 10^6 \text{ s}^{-1}$  (Fig. 5). It is worth noting that the long-range correlations are absent in the parent HDA, they develop during shearing (SI Appendix, Fig. S14B). We interpret that the long-range correlations are a signature of the inflection region between low- and high-density SDAs at  $\dot{\gamma} = 10^6 \text{ s}^{-1}$  (Fig. 2C), akin to those that occur around the Widom line in the absence of shear.

The most surprising prediction of Fig. 4 is that glasses prepared by hyperquenching water from the temperature of maximum density (TMD) to 77 K at infinite cooling rate would have the same  $\rho(p)$  of SDA prepared at the same conditions with a shear rate of about  $\dot{\gamma} = 10^8 \text{ s}^{-1}$ . To test this prediction, we prepare glasses of ML-BOP and TIP4P/Ice by instantaneously changing the target temperature of the corresponding liquids from 280 K to 77 K at 1 bar. SI Appendix, Figs. S20C and S21C show that the density increases suddenly as the target temperature is set to 77 K, settling after a few picoseconds. We define the glass obtained after 10 ps as the “instantaneously quenched glass.” We then produce SDA with the density of the instantaneously quenched glass by shearing LDA at 77 K and 0.1 MPa at rates of  $\dot{\gamma} = 2 \times 10^8 \text{ s}^{-1}$  for ML-BOP and  $\dot{\gamma} = 10^8 \text{ s}^{-1}$  for TIP4P/Ice. Table 2 confirms the prediction of Fig. 4 and further demonstrates that not only the density but also

**Table 2. Comparison of the density and potential energy of ML-BOP and TIP4P/Ice glasses produced by instantaneous hyperquenching from the liquid at 280 K to 77 K at 0.1 MPa and by shearing LDA at 77 K and 0.1 MPa at a rate of  $10^8 \text{ s}^{-1}$  for TIP4P/Ice  $2 \times 10^8 \text{ s}^{-1}$  for ML-BOP**

Model	State	$\rho$ (g cm $^{-3}$ )	$E$ (kJ mol $^{-1}$ )	$E_{IS}$ (kJ mol $^{-1}$ )
ML-BOP	HQG	$1.010 \pm 0.005$	$-39.3 \pm 0.1$	$-40.30 \pm 0.10$
	MDA	$1.010 \pm 0.005$	$-39.3 \pm 0.1$	$-41.10 \pm 0.01$
TIP4P/Ice	HQG	$1.015 \pm 0.001$	$-62.0 \pm 0.1$	$-62.53 \pm 0.23$
	MDA	$1.016 \pm 0.003$	$-62.0 \pm 0.1$	$-63.58 \pm 0.16$

Simulation details are provided in SI Appendix, section III. The error bars in  $\rho$  and  $E$  or HQG were based on the average of 10 independent runs. See also SI Appendix, Tables S2 and S3.

the potential energy of the corresponding instantaneously quenched glass and SDA are indistinguishable. SI Appendix, Figs. S15 and S16 show that this is also the case for their radial distribution functions and response to compression.

Are these very far from equilibrium SDA and HQG also indistinguishable if they have the same  $p, T$ , and  $\rho$ ? While the density of these glasses evolves quite similarly upon aging at constant  $p$  and  $T$  (see SI Appendix, Fig. S15B for ML-BOP and SI Appendix, Fig. S17A for TIP4P/Ice), the potential energies  $E$  of the glasses produced by shearing at  $\sim 10^8 \text{ s}^{-1}$  and instantaneous cooling relax differently (SI Appendix, Figs. S15C and S17B). In all cases,  $E(t)$  decays logarithmically at long times, as previously reported for aging of Lennard-Jones glasses and interpreted to originate from a random walk between increasingly deeper basins in the PEL (51). The short-term evolution of  $E(t)$  is essentially flat for  $\sim 20$  ps for the glasses prepared by shearing while it continuously decreases for those prepared by instant quenching for both the ML-BOP and TIP4P/Ice water models (SI Appendix, Figs. S15C, S17B, S20D, and S21D). The longer lag time of the previously sheared glasses suggests larger barriers between minima in the PEL which and is consistent with the lower energy of the inherent structures  $E_{IS}$  of the MDA sheared at  $\sim 10^8 \text{ s}^{-1}$  compared to  $E_{IS}$  the glasses prepared by instantaneous quenching (Table 2). SI Appendix, section X provides an analysis of the energies, densities, and structure of the inherent structures of MDA, HQG, and liquid. We conclude that these very far from equilibrium amorphous states with same density, temperature, and pressure produced by instantaneous hyperquenching and very high shear rates that do not sample the same region of the PEL: Shearing provides access to states deeper in the potential energy landscape of water.

The agreement in the energy, density, and response to compression of the SDA obtained at  $\sim 10^8 \text{ s}^{-1}$  and instantaneously quenched glasses of ML-BOP and TIP4P/Ice supports that while these glasses are not identical, they are very close despite the extreme conditions at which they were produced. We conclude that the amorphous phase obtained by shearing ice  $I_{h2}$  LDA, or HDA at 0.1 MPa and 77 K at a rate of about  $10^8 \text{ s}^{-1}$  would be a good approximation to the glass that would be achieved by instantaneous quenching of ambient liquid water.

**MDA Recovered from the Experiments Originated in an Amorphous State That Cannot Be Accessed through Hyperquenching of the Liquid.** MDA in the ball-milling experiments was created at uncontrolled and unknown pressures and shear rates, and recovered and analyzed at 0.1 MPa (1). To assess whether MDA recovered from the ball-milling experiment could have originated in the  $\rho(p)$  region only accessible through shearing or have an analog accessible by isobaric hyperquenching (Fig. 4), we first assess the impact of decompression on the density of the sheared phase, and

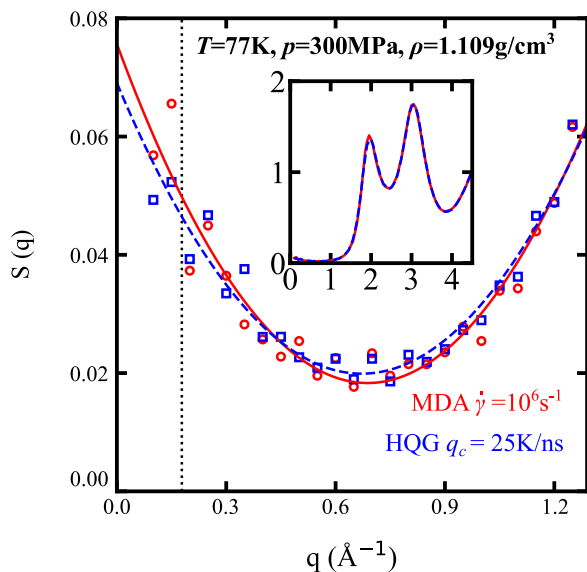


**Fig. 5.** Structure factor  $S(q)$  at  $T = 77 \text{ K}$ ,  $p = 300 \text{ MPa}$ , and  $\rho = 1.109 \text{ g cm}^{-3}$  glass made by isobaric cooling a simulation cell with 64,000 ML-BOP molecules at  $25 \text{ K ns}^{-1}$  (blue squares) and MDA made by shearing a cell of HDA with the same number of molecules at constant shear rate  $\dot{\gamma} = 10^6 \text{ s}^{-1}$  (red circles). The lines represent a fit of a parabola to the data, from which we obtain  $S(0) = 0.076$  for MDA and  $S(0) = 0.069$  for the HQG. The black dotted line indicates  $4\pi/L$ , where  $L = 7 \text{ nm}$  is the box length. The Inset shows that  $S(q)$  of the sheared and hyperquenched amorphous states agree over a larger range of  $q$  values.

**Table 3. Comparison of the enthalpies of MDA and HDA at 77 K in experiments and our simulations with TIP4P/ice**

	Amorphous state	$\rho$ (g cm <sup>-3</sup> )	$H-H_{\text{HDA}}$ (kJ mol <sup>-1</sup> )
Experiments	HDA decompressed to 0.1 MPa <sup>*</sup>	1.17	0
	MDA recovered at 0.1 MPa <sup>†</sup>	1.06 ± 0.06	-0.26 ± 0.20
TIP4P/ice	HDA decompressed to 0.1 MPa <sup>‡</sup>	1.17	0
	MDA prepared at 0.1 MPa and 10 <sup>8</sup> s <sup>-1</sup>	1.00	0
	MDA prepared at 1,000 MPa and 10 <sup>8</sup> s <sup>-1</sup> , then decompressed to 0.1 MPa	1.13	-0.2
	MDA prepared at 300 MPa and 10 <sup>8</sup> s <sup>-1</sup> , then decompressed to 0.1 MPa	1.09	-0.3

Simulation details are provided in *SI Appendix, section III*.

<sup>\*</sup> $\Delta H_{\text{HDA-ice1}} = -2.01 \pm 0.15$  kJ mol<sup>-1</sup>, computed as the sum of  $\Delta H_{\text{HDA-LDA}} = -0.66 \pm 0.01$  kJ mol<sup>-1</sup> (35) and  $\Delta H_{\text{LDA-ice1}} = -1.35 \pm 0.15$  kJ mol<sup>-1</sup> (34, 36).

<sup>†</sup>Obtained from differential scanning calorimetry (1).

<sup>‡</sup>Obtained from the decompression curve of HDA shown in Fig. 2B.

then consider the experimental density of MDA in relation to the extremum of  $\rho_{\text{max}}(p)$  of the line of density maximum predicted by the most recent equation of state (EOS) for supercooled water (42).

Fig. 2B shows that the density of MDAs generated at high pressures and instantly decompressed to 0.1 MPa decreases significantly but remains higher than for MDA created at the same shear rate at ambient pressure: The decompressed sheared amorphous phase retains significant plastic deformation. We expect the same for MDA prepared by ball-milling in the laboratory.

The position  $q_1$  of the first strong peak (FSP) of the structure factor  $S(q)$  of the recovered MDA is in a position intermediate between that of LDA and HDA (1). The simulations uncover an almost linear relationship between  $q_1$  and the density of the amorphous phases generated at  $\dot{\gamma}$  up to 10<sup>8</sup> s<sup>-1</sup> (*SI Appendix, Fig. S11E*). As  $q_1$  of LDA and HDA in ML-BOP are in quantitative agreement with the experiments (*SI Appendix, Fig. S18*), we use  $q_1(p)$  of the model to deduce that for the 1.93 Å<sup>-1</sup> of the FSP of the MDA recovered in the experiments, the density is  $\rho_{\text{rec}}^{\text{MDA}} = 1.07 \pm 0.02$  g cm<sup>-3</sup>, at the center of the 1.06 ± 0.06 g cm<sup>-3</sup> value reported in ref. 1.

Considering that MDA prepared from TIP4P/Ice at 77 K at 300 and 1,000 MPa relaxes 0.05 and 0.14 g cm<sup>-3</sup>, respectively, over a few nanoseconds (orange arrows in Fig. 2B), and that the relaxation of MDA in experiments occurs over several orders of magnitude longer times, we deduce that the recovered MDA with density 1.07 ± 0.02 g cm<sup>-3</sup> originated on a sheared state with density no smaller than ~1.12 g cm<sup>-3</sup>. Fig. 4 supports that such density cannot correspond to a shear-driven phase with a density accessible also by hyperquenching, because 1.12 g cm<sup>-3</sup> is above the highest prediction for the maximum density  $\rho_{\text{max}}(p_{\text{max}}) = 1.08$  g cm<sup>-3</sup> at  $p_{\text{max}} = 151$  MPa along the line of density anomaly of water, according to the latest equations of state based on experimental data (42). We conclude that MDA recovered from the ball-milling experiments is the relaxed form of an amorphous state of water that can only be accessed by shearing.

The shear rates required to reach  $\rho_{\text{rec}}^{\text{MDA}} = 1.07 \pm 0.02$  g cm<sup>-3</sup> at ambient pressure are ~10<sup>10</sup> s<sup>-1</sup> (Fig. 2C), several orders of magnitude larger than those reached during ball-milling (20). The latter is also the case for the larger than 10<sup>8</sup> s<sup>-1</sup> rates needed to access SDAs with density above the line of density maximum of the liquid. We conclude that high pressure, and not extremely high shear rates, is responsible for the high density of the recovered amorphous phase. The white dotted line in Fig. 4 sketches that decompression scenario.

Table 3 shows that MDA produced at 300 and 1,000 MPa with TIP4P/Ice and recovered ambient pressure is 0.2 and 0.3 kJ mol<sup>-1</sup> more stable than HDA, consistent with the 0.26 ± 0.20 kJ mol<sup>-1</sup> we deduced for MDA recovered in the experiments. The agreement in the enthalpies further supports that MDA of ref. 1.

originated from decompression of an amorphous phase produced by shearing—probably at moderate rates—at pressures where HDA would be the most stable amorphous state. We conclude that there is no relation between the MDA produced by ball-milling and the glass that would be produced by instantaneous quenching of ambient liquid water to 77 K.

## Conclusions and Outlook

The discovery of medium-density amorphous ice puzzled the water research community, raising questions about its nature and relationship to LDA, HDA, and the liquid state. Our simulations of shearing of ice  $I_b$  reveal that MDA is not a nanocrystalline state or a mixture of LDA and HDA, but a distinct SDA phase.

SDA prepared at constant shear rate is a nonequilibrium steady-state characterized by time-invariant properties determined only by pressure, temperature, and shear rate. Our simulations support that the nonequilibrium sheared amorphous phases can be prepared directly from LDA, HDA, or any other water glass through ball-milling, effectively eliminating the ice contributions to the measurements.

Modulation of the shear rate results in SDAs with densities that span the entire range from LDA to HDA. The rich phase behavior of solid amorphous water under shear does not conflict with the known polyamorphism of water, but it originates in the extension of the nonequilibrium phase diagram by addition of the shear rate as a new variable. As the shear rate decreases, the properties of the SDA approach those of more stable glasses at the corresponding pressure.

The energy and enthalpy of amorphous solid water increases monotonously with the shear rate, pushing the glass further away from equilibrium. We demonstrate that at pressures above the highest pressure  $p_{\text{max}} = 151$  MPa at which water has a density maximum (42) (or 430 MPa for the ML-BOP water model) the density  $\rho(p, T)$  of amorphous phases accessible through shearing does not overlap with the ones accessible by hyperquenching, irrespective of the shear rate. This lack of overlap in the density of HQG and SDA at high pressures originates on the opposite dependence of the density to shear and cooling rates for water at pressures without a TMD. The implication is that any MDA obtained by ball-milling at pressures above ~150 MPa would be a distinct material without an analog accessible by isobaric hyperquenching of liquid water.

Hyperquenched glasses (HQG) and SDAs prepared at  $p < p_{\text{max}}$  can have the same  $\rho(p, T)$  below the line of density maxima  $\rho_{\text{max}}(p)$ . The simulations reveal that SDA produced with shear rates as high as 10<sup>6</sup> s<sup>-1</sup> and the HQG with identical  $\rho(p, T)$  have indistinguishable structure (including long-range correlations), energy, response to compression and heating, as well as same inherent structure energies that result in almost indistinguishable evolution of density and

energy upon aging. These results suggest that these SDA and HQG sample regions of the potential energy landscape accessible to the liquid in equilibrium and have well-defined fictive temperatures.

The simulations unveil that even very far from equilibrium SDA sheared at  $\sim 10^8 \text{ s}^{-1}$  and the ultrafast cooled glass with identical  $\rho(p, T)$  have indistinguishable enthalpy, structure, and response to compression, and even the same evolution of density on aging. However, they have different inherent structure energies: Simulations with both the ML-BOP and TIP4P/Ice models indicate that the sheared-driven phases are deeper in the potential energy landscape than glasses with same density made by instantaneous quenching. That difference results in slower evolution of the energy of the previously sheared glasses as they age. Considering that the inherent structures of the MDA sheared at rates as high as  $10^6 \text{ s}^{-1}$  are indistinguishable from those of the HQG with same  $\rho(p, T)$ , further studies on the potential energy landscape of SDA as a function of the shear-rate would be highly valuable for understanding the effect of shear deformation on energy barriers and basins.

A corollary of the existence of a line of density maxima, is that the HQG obtained by infinitely fast isobaric cooling of liquid water from the TMD would have the same  $\rho(p, T)$  than an SDA produced at a finite shear rate. The simulations uncover that such rate is around  $10^8 \text{ s}^{-1}$  for both the all-atom TIP4P/Ice and coarse-grained ML-BOP models of water. It is interesting to note that the inverse shear rate  $1/\dot{\gamma}$  corresponds to a time scale of a few nanoseconds, which is comparable to the one found to signal the transition from diffusive to landscape-dominated dynamics in liquids (52).

The similarity in the properties and response to stimuli of the amorphous phase produced by shearing the glasses at  $10^8 \text{ s}^{-1}$  and the glass obtained by instantaneously quenching the liquid from the line of maximum density to 77 K, implies that SDA formed at such rates at 0.1 MPa is a close approximation to the “true” glass state of ambient liquid water made by instantaneous hyperquenching. Ultrafast shear acoustic waves that reach shear rates about  $10^9 \text{ s}^{-1}$  (53) could be used to create these far from equilibrium SDAs in the laboratory.

We interpret the MDA obtained by ball-milling in ref. 1 was generated at pressures above  $\sim 150$  MPa and is a phase accessible only through shearing. Our analysis is based on the density of the recovered MDA in the experiment, which we narrow to  $1.07 \pm 0.02 \text{ g cm}^{-3}$ , and the maximum  $\rho_{\text{max}} = 1.08 \text{ g cm}^{-3}$  along the line of density extrema of water, predicted to occur at  $p_{\text{max}} = 151$  MPa by the most recent equations of state (42). Our analysis of the enthalpy of the amorphous sample recovered at 0.1 MPa, which

we show to be intermediate between the ones of LDA and HDA, supports our interpretation that MDA produced by ball-milling is not related to ambient liquid water.

The existence of a LLT in water remains a focal point for understanding its anomalous behavior (17). Simulations with models such as ML-BOP and TIP4P/Ice that have an LLT are promising to elucidate the fate of this metastable phase transition upon shearing and its interplay with ice crystallization. The contrasting range of densities of SDAs sheared at low and high pressures emphasizes the coupling between density and energy within the two-state thermodynamics model of water, which represents amorphous water phases as a non-ideal mixture of high-density/high-energy and low-density/low-energy motifs (14). However, this study reveals shear-rate dependent density-energy relations in SDA ices distinct from those in LDA and HDA, as well as the smearing of the LLT into a continuous transformation at moderate shear rates and its disappearance upon strong shearing. These findings call for an extension of the formalism of two-state thermodynamics of water to encompass these nonequilibrium stationary states and to elucidate how shearing impacts the LLT and its competition with ice crystallization as the temperature is increased toward and above the glass transition line.

**Data, Materials, and Software Availability.** The datasets for the figures and LAMMPS input files can be accessed and downloaded at <https://doi.org/10.5281/zenodo.13947547> (54). All other data are included in the main text and/or *SI Appendix*.

**ACKNOWLEDGMENTS.** I.d.A.R., D.D., R.K., and V.M. acknowledge support from Air Force Office of Scientific Research through Multidisciplinary University Research Initiative Award FA9550-20-1-0351. S.B and S.K.R.S.S acknowledge support by the Center for Nanoscale Materials, a US Department of Energy (DOE) Office of Science User Facility supported by the US DOE, Office of Basic Energy Sciences under Contract No. DE-AC02-06CH11357. We are grateful to Arnab Neogi for helping in the grain-boundary sliding deformations under load, Eli Martinez for his help on setting the GPUs for our large-scale simulations, and Osamu Mishima for sharing his published data on the extremum of maximum density. We gratefully acknowledge discussions with Jeppe Dyre, Francesco Sciortino, Pablo Debenedetti, Nicolas Giovambattista, Srikanth Sastry, and Kaixin Wang. We thank the Center of High-Performance Computing at the University of Utah for technical support and a grant of computing time.

Author affiliations: <sup>a</sup>Department of Chemistry, The University of Utah, Salt Lake City, UT 84112-0850; <sup>b</sup>Center for Nanoscale Materials, Argonne National Laboratory, Lemont, IL 60439; and <sup>c</sup>Department of Mechanical and Industrial Engineering, University of Illinois, Chicago, IL 60607

1. A. Rosu-Finsen *et al.*, Medium-density amorphous ice. *Science* **379**, 474–478 (2023).
2. D. Mariedahl *et al.*, X-ray scattering and O-O pair-distribution functions of amorphous ices. *J. Phys. Chem. B* **122**, 7616–7624 (2018).
3. T. Loerting, C. Salzmann, I. Kohl, E. Mayer, A. Hallbrucker, A second distinct structural “state” of high-density amorphous ice at 77 K and 1 bar. *Phys. Chem. Chem. Phys.* **3**, 5355–5357 (2001).
4. K. Winkel, D. T. Bowron, T. Loerting, E. Mayer, J. L. Finney, Relaxation effects in low density amorphous ice: Two distinct structural states observed by neutron diffraction. *J. Chem. Phys.* **130**, 204502 (2009).
5. K. Amann-Winkel, D. T. Bowron, T. Loerting, Structural differences between unannealed and expanded high-density amorphous ice based on isotope substitution neutron diffraction. *Mol. Phys.* **117**, 3207–3216 (2019).
6. O. Mishima, L. Calvert, E. Whalley, ‘Melting ice’ at 77 K and 10 kbar: A new method of making amorphous solids. *Nature* **310**, 393–395 (1984).
7. P. Gallo *et al.*, Water: A tale of two liquids. *Chem. Rev.* **116**, 7463–7500 (2016).
8. P. Gallo *et al.*, Advances in the study of supercooled water. *Eur. Phys. J. E* **44**, 143 (2021).
9. C. M. Tonauer, L.-R. Fidler, J. Giebelmann, K. Yamashita, T. Loerting, Nucleation and growth of crystalline ices from amorphous ices. *J. Chem. Phys.* **158**, 141001 (2023).
10. G. D. Pablo, Supercooled and glassy water. *J. Phys. Condens. Matter.* **15**, R1669 (2003).
11. C. A. Angell, Amorphous water. *Ann. Rev. Phys. Chem.* **55**, 559–583 (2004).
12. T. Loerting, N. Giovambattista, Amorphous ices: Experiments and numerical simulations. *J. Phys. Condens. Matter.* **18**, R919 (2006).
13. O. Mishima, H. E. Stanley, The relationship between liquid, supercooled and glassy water. *Nature* **396**, 329–335 (1998).
14. V. Holten, J. C. Palmer, P. H. Poole, P. G. Debenedetti, M. A. Anisimov, Two-state thermodynamics of the ST2 model for supercooled water. *J. Chem. Phys.* **140**, 104502 (2014).
15. V. Holten, D. T. Limmer, V. Molinero, M. A. Anisimov, Nature of the anomalies in the supercooled liquid state of the mW model of water. *J. Chem. Phys.* **138**, 174501 (2013).
16. Z. Yu, R. Shi, H. Tanaka, A unified description of the liquid structure, static and dynamic anomalies, and criticality of TIP4P/2005 water by a hierarchical two-state model. *J. Phys. Chem. B* **127**, 3452–3462 (2023).
17. P. H. Poole, F. Sciortino, U. Essmann, H. E. Stanley, Phase behaviour of metastable water. *Nature* **360**, 324–328 (1992).
18. J. L. F. Abascal, E. Sanz, R. G. Fernández, C. Vega, A potential model for the study of ices and amorphous water: TIP4P/Ice. *J. Chem. Phys.* **122**, 234511 (2005).
19. H. Chan *et al.*, Machine learning coarse grained models for water. *Nat. Commun.* **10**, 379 (2019).
20. F. Shi, T. Napier-Munn, Estimation of shear rates inside a ball mill. *Int. J. Miner. Process.* **57**, 167–183 (1999).
21. L. Pastewka, S. Moser, P. Gumbsch, M. Moseler, Anisotropic mechanical amorphization drives wear in diamond. *Nat. Mater.* **10**, 34–38 (2011).
22. A. Stukowski, Visualization and analysis of atomistic simulation data with OVITO–The open visualization tool. *Model. Simul. Mater. Sci. Eng.* **18**, 015012 (2009).
23. P. M. Larsen, S. Schmidt, J. Schiotz, Robust structural identification via polyhedral template matching. *Model. Simul. Mater. Sci. Eng.* **24**, 055007 (2016).
24. E. B. Moore, E. de la Llave, K. Welke, D. A. Scherlis, V. Molinero, Freezing, melting and structure of ice in a hydrophilic nanopore. *Phys. Chem. Chem. Phys.* **12**, 4124–4134 (2010).
25. I. d. A. Ribeiro, M. d. Koning, Grain-boundary sliding in ice iH: Tribology and rheology at the nanoscale. *J. Phys. Chem. C* **125**, 627–634 (2021).

26. D. Dhabal, R. Kumar, V. Molinero, Liquid-liquid transition and ice crystallization in a machine-learned coarse-grained water model. *Proc. Natl. Acad. Sci. U.S.A.* **121**, e2322853121 (2024).
27. D. Dhabal, S. K. R. S. Sankaranarayanan, V. Molinero, Stability and metastability of liquid water in a machine-learned coarse-grained model with short-range interactions. *J. Phys. Chem. B* **126**, 9881–9892 (2022).
28. J. L. F. Abascal, C. Vega, A general purpose model for the condensed phases of water: TIP4P/2005. *J. Chem. Phys.* **123**, 234505 (2005).
29. D. Dhabal, V. Molinero, Kinetics and mechanisms of pressure-induced ice amorphization and polymorphic transitions in a machine-learned coarse-grained water model. *J. Phys. Chem. B* **127**, 2847–2862 (2023).
30. L. F. Cugliandolo, J. Kurchan, L. Peliti, Energy flow, partial equilibration, and effective temperatures in systems with slow dynamics. *Phys. Rev. E* **55**, 3898 (1997).
31. U. Seifert, T. Speck, Fluctuation-dissipation theorem in nonequilibrium steady states. *Europhys. Lett.* **89**, 10007 (2010).
32. T. E. Gartner III, S. Torquato, R. Car, P. G. Debenedetti, Manifestations of metastable criticality in the long-range structure of model water glasses. *Nat. Commun.* **12**, 3398 (2021).
33. A. Neophytou, F. Sciortino, Potential energy landscape of a coarse grained model for water: ML-BOP. *J. Chem. Phys.* **160**, 114502 (2024).
34. G. P. Johari, G. Fleissner, A. Hallbrucker, E. Mayer, Thermodynamic continuity between glassy and normal water. *J. Phys. Chem.* **98**, 4719–4725 (1994).
35. P. H. Handle, M. Seidl, V. Fuentes-Landete, T. Loerting, Ex situ studies of relaxation and crystallization in high-density amorphous ice annealed at 0.1 and 0.2 GPa: Includes response to: "Comment on: 'Relaxation time of high-density amorphous ice'" by G.P. Johari. *Thermochim. Acta* **636**, 11–22 (2016).
36. R. J. Speedy, P. G. Debenedetti, R. S. Smith, C. Huang, B. D. Kay, The evaporation rate, free energy, and entropy of amorphous water at 150 K. *J. Chem. Phys.* **105**, 240–244 (1996).
37. A. Eltareb, G. E. Lopez, N. Giovambattista, A continuum of amorphous ices between low-density and high-density amorphous ice. *Commun. Chem.* **7**, 36 (2024).
38. M. Utz, P. G. Debenedetti, F. H. Stillinger, Atomistic simulation of aging and rejuvenation in glasses. *Phys. Rev. Lett.* **84**, 1471–1474 (2000).
39. D. J. Lacks, M. J. Osborne, Energy landscape picture of overaging and rejuvenation in a sheared glass. *Phys. Rev. Lett.* **93**, 255501 (2004).
40. V. Viasnoff, F. Lequeux, Rejuvenation and overaging in a colloidal glass under shear. *Phys. Rev. Lett.* **89**, 065701 (2002).
41. P. G. Debenedetti, F. Sciortino, G. H. Zerze, Second critical point in two realistic models of water. *Science* **369**, 289–292 (2020).
42. O. Mishima, T. Sumita, Equation of state of liquid water written by simple experimental polynomials and the liquid-liquid critical point. *J. Phys. Chem. B* **127**, 1414–1421 (2023).
43. A. J. Kovacs, "Transition vitreuse dans les polymères amorphes. Etude phénoménologique" in *Fortschritte der hochpolymeren-forschung* (Springer, 2006), pp. 394–507.
44. S. Mossa, F. Sciortino, Crossover (or Kovacs) effect in an aging molecular liquid. *Phys. Rev. Lett.* **92**, 045504 (2004).
45. N. Giovambattista, F. W. Starr, P. H. Poole, State variables for glasses: The case of amorphous ice. *J. Chem. Phys.* **150**, 224502 (2019).
46. W. Kob, F. Sciortino, P. Tartaglia, Aging as dynamics in configuration space. *Europhys. Lett.* **49**, 590 (2000).
47. N. Giovambattista, H. E. Stanley, F. Sciortino, Cooling rate, heating rate, and aging effects in glassy water. *Phys. Rev. E* **69**, 050201 (2004).
48. F. Sciortino, Potential energy landscape description of supercooled liquids and glasses. *J. Statist. Mech. Theor. Exp.* **2005**, P05015 (2005).
49. T. Hecksher, N. B. Olsen, J. C. Dyre, Fast contribution to the activation energy of a glass-forming liquid. *Proc. Natl. Acad. Sci. U.S.A.* **116**, 16736–16741 (2019).
50. T. E. Gartner, S. Torquato, R. Car, P. G. Debenedetti, Manifestations of metastable criticality in the long-range structure of model water glasses. *Nat. Commun.* **12**, 3398 (2021).
51. L. Angelani, R. Di Leonardo, G. Parisi, G. Ruocco, Topological description of the aging dynamics in simple glasses. *Phys. Rev. Lett.* **87**, 055502 (2001).
52. T. B. Schrøder, S. Sastry, J. C. Dyre, S. C. Glotzer, Crossover to potential energy landscape dominated dynamics in a model glass-forming liquid. *J. Chem. Phys.* **112**, 9834–9840 (2000).
53. T. Pezeril, [INVITED] Laser generation and detection of ultrafast shear acoustic waves in solids and liquids. *Opt. Laser Technol.* **83**, 177–188 (2016).
54. I. de Almeida Ribeiro *et al.*, Data for "Medium-density amorphous ice unveils shear rate as a new dimension in water's phase diagram" (v1.0). Zenodo. <https://doi.org/10.5281/zenodo.13947547>. Accessed 25 October 2024.